International Journal for Multidisciplinary Research (IJFMR)
E-ISSN: 2582-2160 ● Website: www.ijfmr.com ● Email: editor@ijfmr.com

Detection of Ground Glass Opacities in COVID-19 Lung CT Images using Frangi Multiscale Vesselness Measure

Soma Chatterjee[1], Rohit Kamal Chatterjee[2], R T Goswami[3]

[1]Soma Chatterjee, Department of MCA, Techno International Newtown
[2]Rohit Kamal Chatterjee, Department of Computer Science, BIT Mesra
[3]R T Goswami, Department of Computer Science, Techno International Newtown

Abstract
In this work, an automated technique for the quick and accurate detection of Ground Glass Opacities (GGO) in chest CT images of COVID-19 pneumonia patients is presented. The method uses mathematical morphology-based methods and Otsu's thresholding during the segmentation of GGO regions in order to extract the lung fields. The program uses the Frangi Multiscale Vesselness Measure to identify and remove these structures based on the anatomical features of bronchioles. Using a dataset of 155 lung CT images, the study outperformed previous algorithms in terms of sensitivity, specificity, and accuracy, all exceeding 97.22%. Radiologists can be helped by this automated screening method to quickly find GGOs in lung CT scans.

Keywords: Ground Glass Opacities (GGO), COVID-19 pneumonia, Chest CT scans, Mathematical morphology, Frangi Multiscale Vesselness Measure

1. Introduction

By the end of 2019, Wuhan, China had seen multiple cases of pneumonia and the World Health Organization (WHO) declared it a worldwide health catastrophe in December 2019 [1]. The disease-causing virus was soon spread quickly over the world by means of human-to-human transmission.
The most common symptoms associated with COVID-19 are fever, coughing, and exhaustion. Other signs and symptoms include headache, hemoptysis, diarrhea, dyspnea, and lymphopenia [10]. Among the best ways to fight COVID-19, social seclusion is by far the most advised. It is recommended that individuals who exhibit symptoms self-isolate at home for a duration of 14 days, thereby substantially mitigating the likelihood of virus transmission to other individuals. In addition to stopping the virus's transmission, this tactic helps to avoid an excessive number of patients overflowing hospitals. Due to the quick rise in infections, seeking emergency medical attention at the same time for everyone who is ill may result in overcrowding in hospitals and a greater death toll [5].
One of the most important tools for communicating important artifacts to medical specialists is computed tomography (CT). The different patterns of COVID-19 tomographic presentations present a challenging problem, especially for physicians who have to diagnose a lot of CT images in a day or two. In addition, medical professionals need to make use of established guidelines and calculate the degree of pulmonary damage brought on by COVID-19 infection in order to make a diagnosis and provide a treatment plan.

Monitoring the disease's progression is an additional important factor to take into account. Experts need to measure results both before and after therapy, mostly to assess how well the treatment worked.[6]

A complex and difficult situation is presented by the clinical characteristics of COVID-19, which are marked by a high rate of transmission and odd early signs [7]. Ground Glass Opacity (GGO) is a common lesion in COVID-19, and important diagnostic details including the size, shape, and texture of the GGO help physicians treat patients in a timely manner [2, 3]. The variety of GGO features, such as their quantity, kind, form, size, density, and position, differs greatly between patients [4].

When making a diagnosis, physicians encounter difficulties impacted by things like insufficient experience, diversions, or exhaustion, which can lead to COVID-19 misdiagnoses [5, 6]. These difficulties can be lessened by accurately segmenting GGO from CT scans in the early stages of COVID-19. If successful, this kind of segmentation allows for the adoption of appropriate predictions and treatment plans, which might lead to an 80% reduction in infection rates [7]. Therefore, early and reliable GGO identification is essential for a proper COVID-19 diagnosis and course of treatment.

Interestingly, Ground Glass Opacity (GGO) can also appear in CT scans of various lung conditions, including cancer, bacterial or viral pneumonia, and widespread respiratory disorders [4]. It is not limited to COVID-19 pneumonia. GGO usually does not affect the texture of the bronchi or arteries, but instead appears on CT images as an increased attenuation suspended mass with cloud-like features [3].

Determining the malignancy of non-solitary nodules requires accurate determination of the GGO growth rate. However, because of their hazy borders or margins, different GGO forms are difficult to segment and analyze [6].

This paper proposes an efficient and automated algorithm for rapidly segmenting GGO in chest CT images, frequently observed in nCOVID-19 Pneumonia cases. Such an automated screening approach would significantly benefit radiologists by facilitating quick and accurate anomaly detection in chest CT images.

- An effective filling technique based on mathematical morphology and Otsu's thresholding are used to segment the lung fields in chest CT scans. This method produces a mask (ROI) that precisely removes the lung region.
- The segmentation process considers the anatomy of bronchioles and vessels to detect these structures. Given that larger bronchioles and vessels are elongated structures, Frangi's vesselness measure is applied to identify and eliminate them from the final result.
- Segmentation of regions containing GGO is challenging due to their lack of well-defined borders. We addressed this challenge by focusing on the distinct pathological appearance of GGO, characterized by intensity variation from the surrounding lung tissue. This is achieved by eliminating structures other than GGO regions in the lung field.

The remainder of the paper is structured as follows: Section II provides a detailed description of our proposed algorithm, followed by a concise overview of Frangi Vesselness Filtering theory [2]. In Section III, we showcase the results obtained by applying our algorithm to various images. We evaluate the performance of our proposed algorithm by comparing it with other proposed algorithms, and the findings are presented in this section.

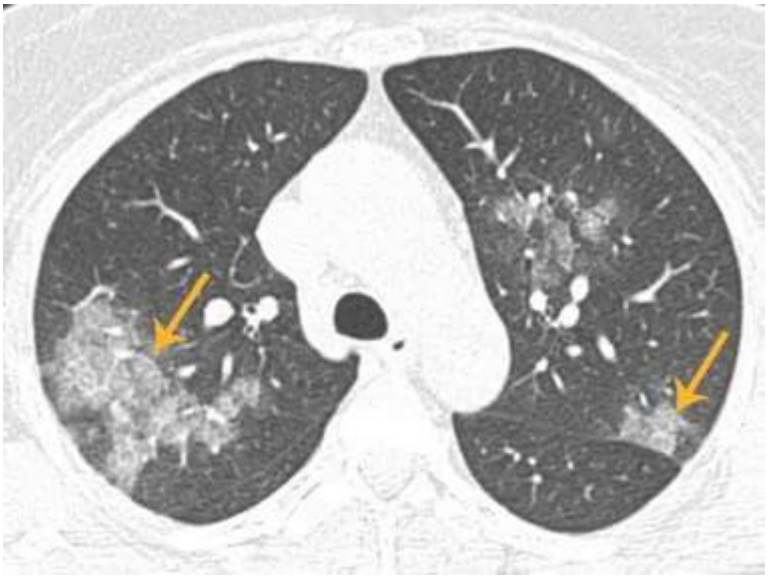

Figure 1: The structure of COVID-19 lung CT images including lung background (black area) and GGO has been shown by yellow arrows as above (Source: https://images.app.goo.gl/4vDYpZdzhvNvJN1J6)

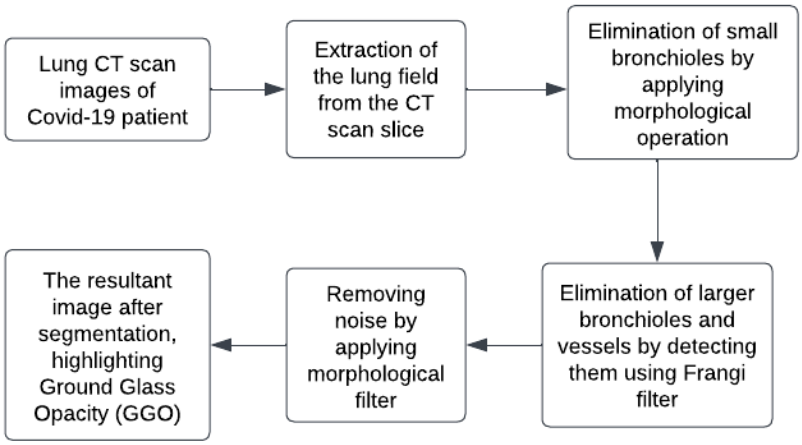

Figure 2: Block Diagram of the proposed algorithm

2. Related Work:

The three main types of work that are most relevant to our research are discussed in this section: (1) Using deep learning networks for segmenting Ground Glass Opacity (GGO). (2) GGO segmentation techniques devoid of deep neural network integration. (3) Developments in artificial intelligence for COVID-19 detection.

2.1. Deep Learning in Segmentation of Lung Diseases:

A growing number of deep neural networks have been proposed for lung GGO segmentation in response to the COVID-19 pandemic. There are three primary types for these solutions. First, deep neural networks with an attention mechanism trained by a fundamental information constraint, such as Inf-net, which performs network training to segment GGO areas in chest CT by extracting low-level semantic features

earlier [7, 17]. Important strategies include segmenting infected GGO regions by joining interactive attention-thinning and attention-rejecting networks [18]. Improved feature map segmentation, expanded convolution residual attention blocks, and improved receptive fields are a few more effective approaches [19]. These techniques focus on using known data as a constraint to improve network training [20], but they have trouble segmenting contours because of fuzzy edges brought on the poor contrast between the lung background and GGO areas.

The goal of the second class of deep segmentation techniques is to improve CT image quality. A novel data augmentation technique based on Gabor filter and convolutional deep learning for upgrading COVID-19 images [22], the application of multi-scale feature image fusion and enhancement networks [21], and the employment of Dense GAN and multi-layer attention to segment GGO [23] are a few examples.

In the third category, attention mechanisms and image enhancement are combined. Sugeno fuzzy integral-based CNN, for example, is used to detect GGO in COVID-19 [24], while Anam-net, which has been enhanced by a lightweight CNN, is used for GGO segmentation [25, 26]. Notably, feature selection based on ant colony and particle swarm optimization algorithms can also be used in the identification of GGO [27]. It is important to recognize, nonetheless, that deep neural networks are trained under the supposition of a small amount of prior knowledge and improved image quality [28]. Therefore, large computation to train these dense networks may not be required when prior information is sufficient [29].

2.2. Non-network in segmentation of lung diseases:

Deep neural networks are not the only option; non-network techniques have also shown promise in the segmentation of lung ground glass opacity (GGO). Compared to deep neural networks, which use a unified approach, non-network models usually involve two different tasks: segmenting lung contours and GGOs. Methods based on morphological operations [30], threshold segmentation in combination with Gabor filter [31], and automatically segmenting abdominal CT volumes into many organs using locally linear embedding graph segmentation [32] have demonstrated quick and precise outcomes for lung contour segmentation.

Several techniques are used in non-network methods to segment the GGO area: (1) Local segmentation tasks, which include acquiring and combining lung nodule regions, are separated into global tasks [33]. (2) For the purpose of lung nodule segmentation, image features are improved by raising image resolution [34]. (3) Support vector machines are integrated with features to segment lung cancer cases [35]. In contrast to deep learning methods, non-network methods frequently use different algorithms for the two segmentation tasks: GGO segmentation and lung contour segmentation [36].

The difficulty of selecting the best parameters is an ongoing concern with non-network methods, despite their benefits [37]. Difficulties arise when choosing the operator size in image preprocessing and choosing the proper segmentation sites in threshold segmentation [33, 38]. Interestingly, non-network approaches frequently perform well for quick pixel segmentation without requiring a lot of training [39]. When compared to deep learning, threshold-based segmentation—which is employed in these methods—has shown superior performance in lung contour segmentation, taking into account the modification in the relation between shape and position.

However, the accuracy of CT image GGO segmentation using threshold approaches is limited by non-network methods, mostly due to difficulties in parameter selection. This finding encourages research into a novel strategy in which segmentation automatically modifies its parameters according to the quality of the image. During the GGO segmentation of lung CT images, an extensive amount of preparatory

information is provided, including one-dimensional CT rapid lung cavity localization [5], pneumonia characteristic information [40], and more. By using these various parameters as initial data, a mapping relationship between input images and segmentation parameters can be created.

2.3. AI progresses for COVID-19:

There has been significant use in COVID-19 diagnosis in the field of AI advancement, especially with methodologies characterized by the previously mentioned automatic segmentation techniques. These developments have shown to be successful in a number of applications, such as monitoring a patient's condition progression, enabling follow-up therapies, and diagnosing suspicious patients [7, 41, 42]. In order to fully understand a patient's individual circumstances, it is essential to segment the Ground Glass Opacity (GGO) zones in CT scans. When diagnosing suspected cases, deep neural evolution algorithms allow for direct examination of whether a patient is affected or not.

For instance, Convolutional Neural Networks (CNN) and dynamic feature selection can be used to diagnose pneumonia based on architecture, which includes confirmed COVID-19, confirmed viral, and confirmed bacterial cases. These strategies' predictive power for COVID-19 is in good alignment with radiologists' diagnostic skills. Furthermore, segmentation provides quantitative findings that are useful for determining the infection status [43, 44]. For example, a patient information cloud system and an intelligence analytic system based on local binary patterns help physicians make more accurate diagnoses and provide better follow-up care.

In summary, supported by efficient segmentation techniques, AI significantly enhances the diagnostic capabilities for COVID-19 [45].

With accuracy rates of 96.09% and 98.09%, respectively, Zargari et al. [3] presented a machine learning technique that successfully categorizes chest x-ray pictures into COVID-19 patient and non-COVID-19 person classes. The features that were retrieved utilizing novel Fractional Multichannel Exponent Moments (FrMEMs) from the chest x-ray pictures.

Zhu et al. [4] obtained average sensitivity, specificity, and accuracy for AMAP-based GGO segmentation results of 86.94%, 94.33%, and 94.06%, respectively. Markov assessed the performance based on the subjective assessment of radiologists as well as quantificational analysis and diagnosis.

The Inf-Net deep network, developed by Fan DP et al. [8], overcomes the state-of-the-art models in use today and advances the state-of-the-art in this field by efficiently detecting COVID-19 lung infections from chest CT scans.

According to Zhou et al. [12], a deep learning-based model can accurately identify COVID-19 pneumonia on high-resolution CT scans, increasing radiologists' productivity and cutting down on reading time by 65%.

A deep learning-based algorithm that efficiently diagnoses COVID-19 pneumonia on high-resolution CT was presented by Song Y et al. [31], increasing radiologists' productivity and cutting down on reading time by 65%. With the use of a deep learning-based model, radiologists can more efficiently identify COVID-19 pneumonia on high-resolution CT scans, saving them 65% of the reading time.

In order to improve computational complexity and performance over previous techniques, Sinaga Kristina [32] et al. created the U-k-means clustering algorithm, which automatically determines an ideal number of clusters without initialization or parameter selection.

3. Methodology

A binary mask is made to separate the lung region from its background using mathematical morphology-based filling approaches and Otsu's automatic thresholding. Small bronchioles and arteries are then eliminated by using the appropriate mathematical morphology-based filters. Ground Glass Opacities (GGOs), vessels, and bigger bronchioles are the only remaining objects in the final image. To differentiate GGOs from these elongated items, Frangi's vesselness measure [2] is utilized, taking into account the tubular features of bronchioles and vessels. Frangi's filter defines a vesselness measure for each pixel by using the eigenvalues of the Hessian matrix, making it possible to identify tubular structures in an image, shown later. This metric shows the probability that a pixel is a portion of a GGO or bronchiole.

After applying a threshold and the Frangi filter to the image, a binary image that only includes the vessels and bronchioles is produced. This image's inverse is used as a mask to remove the veins and bronchioles. Lastly, to get rid of any last bits of noise and small artifacts, morphological techniques like median and opening filters are used. Only the areas of the CT scan image that included GGOs are included in the final image.

2.1 Extraction of Lung field:

Looking at Fig. 1, the background and lung have lower grey values than the surrounding muscles, heart, and bones. Consequently, all that is needed to separate these entities in a CT scan slice is an Otsu's threshold. After the binary image is inverted, the holes are filled using a morphological hole-filling technique, which also creates a mask that may be used to extract the Region of Interest (ROI). The lung field can then be extracted more easily by multiplying this binary mask by the original image.

2.2 Elimination of Small Bronchioles

Because of the partial volume effect, bronchioles and arteries in the lung CT scan slice frequently show as little white spots. Disc structuring elements with a radius of three pixels are used in morphological erosion processes that eliminate these distributed bronchioles, which appear as high-intensity oval objects. After that, an object-enhancing White Top-Hat Transform is applied to the final image.

2.3 Elimination of Larger Bronchioles and Vessels

After removing small bronchioles, the remaining structures in the lung field include tubular-shaped (elongated) bronchioles and vessels, along with cloud-like suspended GGOs with no defined boundaries. To eliminate bronchioles and vessels from the lung field, they must be identified based on their anatomical structures. Frangi's vesselness measure [2] is a well-known tool for detecting elongated tubular structures. This research effectively segmented vessels and bronchioles using Frangi's vesselness measure. Following this, these tubular structures were removed from the lung field, leaving behind the GGO regions and a small amount of residual noise.

The explanation that follows goes into further detail about the Frangi filter's application in the identification of arteries and bronchioles. The first stage involves computing a Hessian matrix at each image pixel at a specific scale, s. The Hessian matrix for a two-dimensional input image is a two-by-two matrix made up of second-order partial derivatives of the intensity at a point specified by the equation that follows:

$$\nabla^2 I(x,y) = \begin{bmatrix} \frac{\partial^2 I(x,y)}{\partial x^2} & \frac{\partial^2 I(x,y)}{\partial x \partial y} \\ \frac{\partial^2 I(x,y)}{\partial y \partial x} & \frac{\partial^2 I(x,y)}{\partial y^2} \end{bmatrix} \quad (1)$$

In practice, the second-order partial derivatives of input image I at a point (x, y) is defined as a convolution of Gaussian with the derivative at scale s as given by the equation:

$$\frac{\partial I(x,y,s)}{\partial x} = s^{\gamma} I(x,y) * \frac{\partial G(x,y,s)}{\partial x} \quad (2)$$

where G(x, y, s) denotes a Gaussian convolution kernel at scale s with a parameter γ and is defined by the following equation:

$$G(x,y,s) = \frac{1}{\sqrt{(2\pi s^2)}} \exp\left(-\frac{x^2 + y^2}{2s^2} \right) \quad (3)$$

To identify the tubular structures from their background, Frangi et al. [5] proposed the following vesselness measure:

$$v_0(s) = \begin{cases} 0 & \text{if } \lambda_2 > 0 \\ \exp(-\frac{R_\beta^2}{2\beta^2})(1 - \exp(-\frac{S^2}{2c^2})) \end{cases} \quad (4)$$

where β and c are two user defined parameters to control the amount of importance affirmed on R_β and S.

Here, $R_\beta = \frac{\lambda_1}{\lambda_2}$ is the blobness measure in 2D and accounts for the eccentricity of the second order ellipse, where λ_1 and λ_2 the eigenvalues of the 2-D Hessian Matrix. In order to reduce the response of the background pixels, Frangi et al. used the Frobenius norm $S = \sqrt{\lambda_1^2 + \lambda_2^2}$ of the Hessian matrix in equation (4). The eigenvalues and eigenvectors of the Hessian matrix are closely related to the intensity and direction of the tubular structure. The relation between the eigenvalues λ1 and λ2 is summarized in Table 1 with the possible patterns in 2- D, depending on the value of the eigenvalues λ_k (H=high, L=low, usually small, +/- indicate the sign of the eigenvalue). The eigenvalues are ordered: $|\lambda_1| \leq |\lambda_2|$. As the bronchioles and vessels are bright objects, λ_1 should take a low (L) value compared to a high negative (H-) values of λ_2, therefore, equation (4) ignored the negative values of λ_2. The vesselness measure in Equation (4) is calculated at a specific scale, s. The final estimate of the measure is decided on the maximum response available at a pixel as described in Equation (5) below:

$$\upsilon_0(\gamma) = \max_{s_{min} \leq s \leq s_{max}} \upsilon_0(s, \gamma) \quad (5)$$

where s_{min} and s_{max} are constant decided on the minimum and maximum scale in which the structures are expected to be found. Frangi's vesselness measure correctly segments the bronchioles and vessels from the lung field, and the inverse of this image is used as a mask to eliminate these structures.

Table 1: Possible Patterns in 2D

λ_1	λ_2	Orientation Pattern
N	N	Noisy
L	H-	Tubular Bright

L H-	H+ H-	Tubular Dark Blob like bright
H+	H+	Blob like dark

Table 1. represents possible patterns in 2D, depending on the value of the eigenvalues λ_k (H=high, L=low, usually small, +/- indicate the sign of the eigenvalue). The eigenvalues are ordered: $|\lambda_1| \leq |\lambda_2|$

2.4 Removing Noise

Only the GGOs are left in the lung field after the bronchioles and other elongated structures have been removed. After that, this image is binarized using local Otsu thresholding to identify the locations of GGOs. However, certain dispersed noisy objects are produced during the binarization process. This is addressed by removing these small artifacts using a median filter. To get the segmented GGO zones, multiply the binary mask that results with the original CT image.

3. Dataset collection

A diverse dataset of about 7000 chest CT images was compiled from Kaggle repository. This dataset included 1500 normal lung CT scans from the LIDC dataset.

Dataset link https://www.kaggle.com/c/siim-covid19-detection?utm_medium=email&utm_source=gamma&utm_campaign=comp-siim-covid19

4. Results and Discussions

6,594 lung CT scans from 155 COVID-19 patients make up our experimental image collection; the scans were taken from the publicly accessible Kaggle dataset [25]. The Ground Glass Opacities (GGO) were manually drawn by a trained radiologist for our algorithm's performance estimate and comparison. The results of using our method on chest CT scans are shown in this part, along with a quantitative comparison of its performance to recently proposed algorithms.

Here are four sample CT slices and the accompanying outputs of our algorithm from a 51-year-old COVID-positive patient. The final images only show the GGO and have no background noise.

The original chest CT scan images are shown in Figure 3a, where the lung region is darker than the muscles, bones, and heart. To extract the lung field (Region of Interest, or ROI), Otsu's thresholding technique and a morphological filling algorithm first design a mask (Figure 3b). Using the mask produced in the algorithm's initial phase, the ROI effectively eliminates the background and highlights any bright objects. Smaller vessels are deleted, which tend to seem darker due to the partial volume effect, by eroding the image using a disk-shaped structural element. The resultant image is then enhanced using a white Top-Hat transform, as described in Step 2 (section 2).

The improved image generated by the Frangi filter, which identifies vessel-like bronchioles and other elongated features, is shown in Figure 3c. The filtered image is then thresholded using a local Otsu's threshold to produce a binary mask. On the binary mask, morphological dilation is used to link nearby GGO regions.

In Figure 3d, linked structures outside of the lung regions are eliminated by combining the lung mask with the complement of the dilated binary mask. To further lessen noise in the final GGO segmentation, a median filter is used. Only the GGO zones are segregated in Figure 2e, which displays the final result. To create the final GGO segmentation image, the binary GGO segmentation is multiplied by the original clipped image.

Sample CT slices from a 51-year-old COVID-19 patient are shown in Figure 4, along with the matching algorithm outputs. The resulting images remove all background noise and successfully extract the GGO areas. We evaluated our algorithm under a variety of situations, including CT scans from patients with diffuse respiratory diseases, to see how well it segmented GGO in lung CT scans.

To evaluate the performance of our segmentation algorithm, we calculated the sensitivity (SE), specificity (SP), and accuracy (AC). These measures are defined as follows:

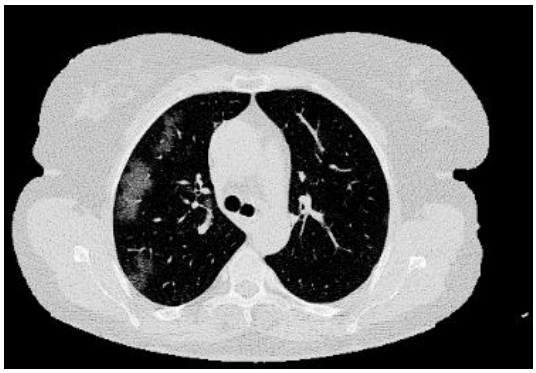

(a)

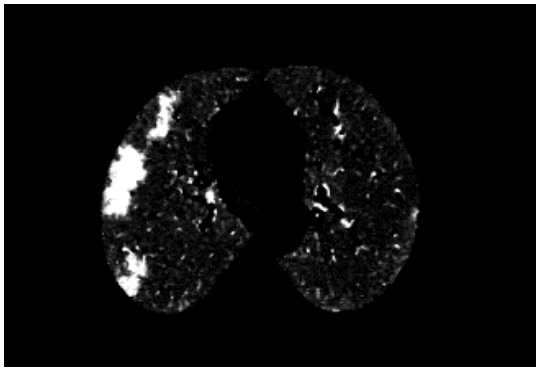

(b)

(c)

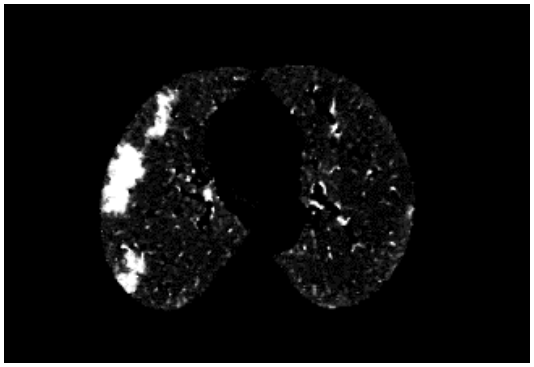

(d)

(e)

Fig. 3: Experimental results of the proposed algorithm on a chest CT image; (a) Original Image; (b) Binary Mask of Lung Region; (c) Bronchioles & Vessel Segmentation using Frangi vessel segmentation; (d) Segmented Image with noise; (e) Binary mask ; (f) Final segmented Image

(a)Input 1

(b) Output 1

(c) Input 2

(d) Output 2

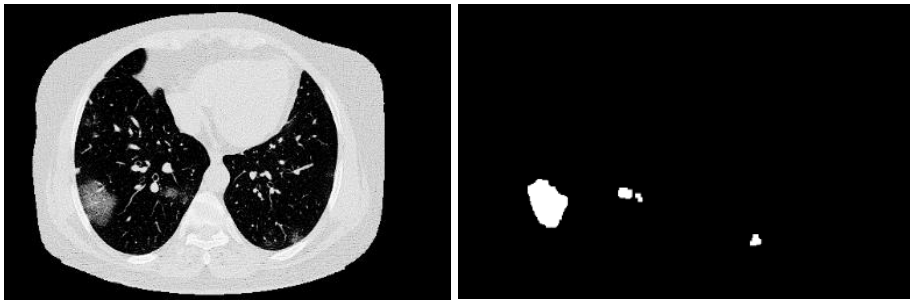

(e) Input 3 (f) Output 3

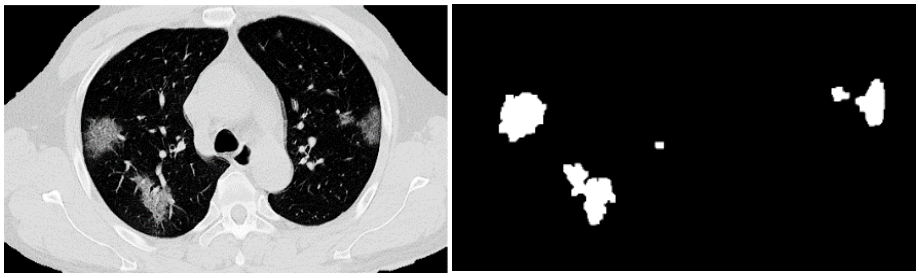

(g) Input 4 (h) Output 4

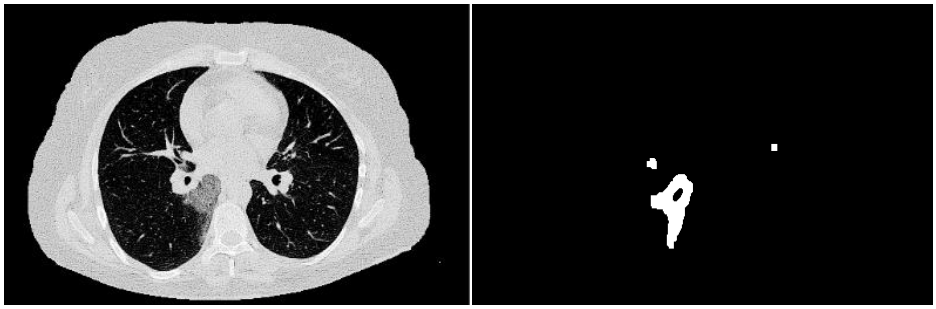

(i) Input 4 (j) Output 4

Fig. 4: Final inputs and outputs of 4 CT slices of a 51-year-old Covid positive patient

$$\text{Sensitivity} = \frac{\text{TP}}{\text{P}}$$

$$\text{Specificity} = \frac{\text{TN}}{\text{N}}$$

$$\text{Accuracy} = \frac{(\text{TP}+\text{TN})}{\text{AreaOfLung}}$$

Here, TP represents the number of pixels correctly classified as GGO regions, and TN represents the number of pixels correctly classified as non-GGO regions. The area of actual GGO regions is denoted as P, while the total area of non-GGO regions is denoted as N. To establish the ground truth for evaluation, an expert radiologist manually marked the regions of GGO on the actual images using a digital pen. The sum of P and N represents the total lung area. Table 2 compares the performance of the recently proposed algorithms with our algorithm.

Table 2: Comparison of the proposed method with the existing method

Algorithms	Sensitivity %	Specificity %	Accuracy %
Yanjie Zhu et al. [4]	89.98	97.59	97.40
Hassanien AE.et.al [5]	95.27	99.70	97.48
Diniz. et al. [28]	95.00	96.00	93.50
Ali RMM.et.al [30]	90.00	70.00	80.00
Thomas.et.al [6]	94.00	92.00	93.00
Jones.et.al [7]	95.00	93.00	94.00
A Gupta et al [29]	95.00	93.00	94.00
Chen. et al [12]	96.00	94.00	95.00
Our Result	96.89	95.23	97.22

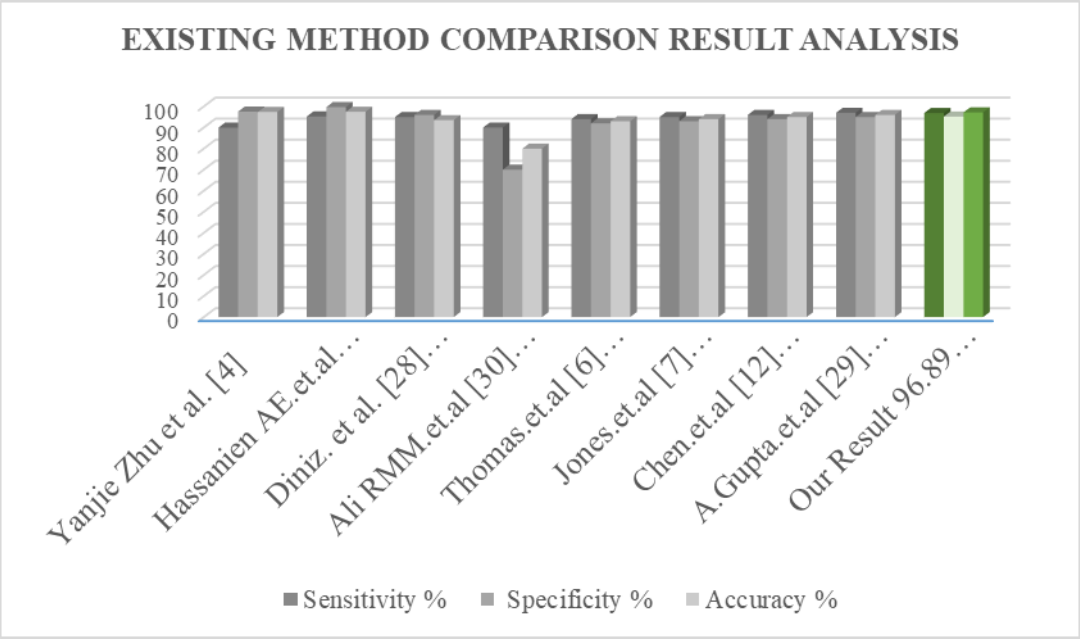

Fig. 5: Result Analysis & Comparison

5. Conclusion and Future Work

Using Frangi Multilevel Filtering and Mathematical Morphology approaches, we have developed a robust algorithm for ground-glass opacity (GGO) segmentation in lung CT scan images of COVID-19 patients. Our methodology's evaluation has shown that it is effective in both efficiently detecting regions containing GGO and properly segmenting lungs from chest CT images. With average sensitivity, specificity, and accuracy of 96.89%, 95.23%, and 97.22%, respectively, the algorithm performs well. This segmentation technique outperforms previous methods in terms of complexity and time consumption, providing radiologists with a useful and workable alternative to help them detect GGO in COVID-19 pneumonia cases.

Our algorithm's success motivates more improvements and wider applications to be thought of:

Extension to Identify Consolidations: The algorithm's reach can be extended to identify consolidations that appear in COVID-19's subsequent phases. This modification would make it easier to analyze how a

disease develops more thoroughly, which would help identify cases that are severe and allow for quick medical intervention. Our approach, which was first created for COVID-19, has potential for use in more extensive medical settings. Through optimization of GGO detection, the system can be modified to recognize analogous patterns in CT scans that are suggestive of several illnesses, such as pneumonia and cancer. This more comprehensive approach will greatly aid in the timely and precise diagnosis of many respiratory and lung-related illnesses.

As we advance, taking care of these issues will improve the algorithm's COVID-19 diagnosing skills as well as its applicability to a larger spectrum of medical imaging problems. The basis for future studies and developments in the automated processing of chest CT images for better clinical decision support is laid by this flexible and scalable method.

6. Acknowledgement

We extend our sincere appreciation to Dr. Asit Sen for graciously providing assistance during the validation process of Ground Glass Opacities (GGO) in lung CT scan images of COVID-19 patients.

7. References

1. Worldometers. (2021). COVID Live - Coronavirus Statistics - Worldometer. Retrieved from https://www.worldometers.info/coronavirus/
2. Frangi, A.F., Niessen, W.J., Vincken, K.L., Viergever, M.A. (1998). Multiscale vessel enhancement filtering. In: Wells, W.M., Colchester, A., Delp, S. (eds) Medical Image Computing and Computer-Assisted Intervention - MICCAI'98. MICCAI 1998. Lecture Notes in Computer Science, vol 1496. Springer, Berlin, Heidelberg. https://doi.org/10.1007/BFb0056195
3. Zargari Khuzani, A., Heidari, M., & Shariati, S.A. (2021). COVID-Classifier: an automated machine learning model to assist in the diagnosis of COVID-19 infection in chest X-ray images. Sci Rep 11, 9887. https://doi.org/10.1038/s41598-021-88807-2
4. Zhu Y, Tan Y, Hua Y, Zhang G, Zhang J. (2012). Automatic segmentation of ground-glass opacities in lung CT images by using Markov random field-based algorithms. J Digit Imaging, 25(3), 409-22. https://doi.org/10.1007/s10278-011-9435-5
5. Salem Hareedy M, Rashad SM, Hetta HF, Hassanien SM, Abdellatif H, Hassanien M. (2021). CYP2D6 and CYP3A4 variants influence the risk and outcome of COVID-19 infection among rheumatoid arthritis patients maintained on hydroxychloroquine. Drug Metab Pers Ther. https://doi.org/10.1515/dmdi-2020-0164
6. Thomas C, Shilton S, Thomas C, Iye CM, Martínez-Pérez GZ. (2022). COVID-19 self-testing, a way to "live side by side with the coronavirus": Results from a qualitative study in Indonesia. PLOS Glob Public Health, 2(10), e0000514. https://doi.org/10.1371/journal.pgph.0000514
7. Jones VG, Mills M, Suarez D, Hogan CA, Yeh D, Segal JB, Nguyen EL, Barsh GR, Maskatia S, Mathew R. (2020). COVID-19 and Kawasaki Disease: Novel Virus and Novel Case. Hosp Pediatr, 10(6), 537-540. https://doi.org/10.1542/hpeds.2020-0123
8. Fan DP, Zhou T, Ji GP, Zhou Y, Chen G, Fu H, Shen J, Shao L. (2020). Inf-Net: Automatic COVID-19 Lung Infection Segmentation From CT Images. IEEE Trans Med Imaging, 39(8), 2626-2637. https://doi.org/10.1109/TMI.2020.2996645
9. Pádraig Cunningham, Matthieu Cord, and Sarah Jane Delany. (2008). Supervised learning. In Machine learning techniques for multimedia: case studies on organization and retrieval. Springer, 21–49.

10. Shah FM, Joy SKS, Ahmed F, Hossain T, Humaira M, Ami AS, Paul S, Jim MARK, Ahmed S. (2021). A Comprehensive Survey of COVID-19 Detection Using Medical Images. SN Comput Sci, 2(6), 434. https://doi.org/10.1007/s42979-021-00823-1
11. Digital image processing, author=Gonzalez, Rafael C, year=2009, publisher=Pearson education india.
12. Zhou L, Li Z, Zhou J, Li H, Chen Y, Huang Y, Xie D, Zhao L, Fan M, Hashmi S, Abdelkareem F, Eiada R, Xiao X, Li L, Qiu Z, Gao X. (2020). A Rapid, Accurate and Machine-Agnostic Segmentation and Quantification Method for CT-Based COVID-19 Diagnosis. IEEE Trans Med Imaging, 39(8), 2638-2652. https://doi.org/10.1109/TMI.2020.3001810
13. Supervised learning, author=Cunningham, Pádraig and Cord, Matthieu and Delany, Sarah Jane, booktitle=Machine learning techniques for multimedia: case studies on organization and retrieval, pages=21–49, year=2008, publisher=Springer.
14. Yiwei Wang, Lei Deng, Lianyu Zheng, Robert X. Gao, Temporal convolutional network with soft thresholding and attention mechanism for machinery prognostics, Journal of Manufacturing Systems, Volume 60, 2021, Pages 512-526, ISSN 0278-6125, https://doi.org/10.1016/j.jmsy.2021.07.008.
15. Peng, Joanne & Lee, Kuk & Ingersoll, Gary. (2002). An Introduction to Logistic Regression Analysis and Reporting. Journal of Educational Research, volume 96, Pages 3-14. https://doi.org/10.1080/00220670209598786
16. Christian Leistner, Amir Safavi, Jakob Santner, and Horst Bischof. (2009). Semi-supervised random forests. In 2009 IEEE 12th international conference on computer vision. IEEE, 506–513.
17. Vladimir Nasteski. (2017). An overview of the supervised machine learning methods. Horizons, 4 (2017), 51–62.
18. Nastaran Enshaei, Anastasia Oikonomou, Moezedin Javad Rafee, Parnian Afshar, Shahin Heidarian, Arash Mohammadi, Konstantinos N Plataniotis, and Farnoosh Naderkhani. (2022). COVID-rate: an automated framework for segmentation of COVID-19 lesions from chest CT images. Scientific Reports, 12(1), 3212.
19. Kristina P Sinaga and Miin-Shen Yang. (2020). Unsupervised K-means clustering algorithm. IEEE access, 8 (2020), 80716–80727.
20. Kushal Virupakshappa and Erdal Oruklu. (2019). Unsupervised machine learning for ultrasonic flaw detection using Gaussian mixture modeling, k-means clustering and mean shift clustering. In 2019 IEEE International Ultrasonics Symposium (IUS). IEEE, 647–649.
21. Sanghoon Lee and Melba M Crawford. (2005). Unsupervised multistage image classification using hierarchical clustering with a Bayesian similarity measure. IEEE Transactions on Image Processing, 14(3), 312–320.
22. Syrjala H, Broas M, Ohtonen P, Jartti A, Paakko E. (2017). Chest magnetic resonance imaging for pneumonia diagnosis in outpatients with lower respiratory tract infection. Eur Respir J, 49(1), 1601303. https://doi.org/10.1183/13993003.01303-2016
23. Diletta Cozzi, Edoardo Cavigli, Chiara Moroni, Olga Smorchkova, Giulia Zantonelli, Silvia Pradella, and Vittorio Miele. (2021). Ground-glass opacity (GGO): a review of the differential diagnosis in the era of COVID-19. Japanese journal of radiology, 39(8), 721–732.
24. Raghubir S Khedar, Rajeev Gupta, Kartik Mittal, Alok Mathur, Jugal B Gupta, Yogendra Singh, Swati Sharma, and Krishna K Sharma. (2023). Greater COVID-19 Severity and Mortality in Hospitalized Patients in the Delta-phase Compared to the Others: A Single Center Prospective Registry. The Journal of the Association of Physicians of India, 71(7), 11–12.

25. Kaggle: Your machine learning and data science community. (2010). author=Goldbloom, A and Hamner, B.
26. Automatic X-ray COVID-19 Lung Image Classification System based on Multi-Level Thresholding and Support Vector Machine Lamia Nabil Mahdy, Kadry Ali Ezzat, Haytham H. Elmousalami, Hassan Aboul Ella. (2020). https://doi.org/10.1101/2020.03.30.20047787
27. Apostolopoulos ID, Aznaouridis SI, Tzani MA. (2020). Extracting Possibly Representative COVID-19 Biomarkers from X-ray Images with Deep Learning Approach and Image Data Related to Pulmonary Diseases. J Med Biol Eng, 40(3), 462-469. https://doi.org/10.1007/s40846-020-00529-4
28. Diniz JOB, Quintanilha DBP, Santos Neto AC, da Silva GLF, Ferreira JL, Netto SMB, Araújo JDL, Da Cruz LB, Silva TFB, da S Martins CM, Ferreira MM, Rego VG, Boaro JMC, Cipriano CLS, Silva AC, de Paiva AC, Junior GB, de Almeida JDS, Nunes RA, Mogami R, Gattass M. (2021). Segmentation and quantification of COVID-19 infections in CT using pulmonary vessels extraction and deep learning. Multimed Tools Appl, 80(19), 29367-29399. https://doi.org/10.1007/s11042-021-11153-y
29. Jain, R., Gupta, M., Taneja, S. et al. (2021). Deep learning based detection and analysis of COVID-19 on chest X-ray images. Appl Intell, 51, 1690–1700. https://doi.org/10.1007/s10489-020-01902-1
30. Ali RMM, Ghonimy MBI. (2020). Semi-quantitative CT imaging in improving visualization of faint ground glass opacities seen in early/mild coronavirus (COVID-19) cases. Egypt J Radiol Nucl Med, 51(1), 244. https://doi.org/10.1186/s43055-020-00354-4
31. Amir Hossein Barshooi, Abdollah Amirkhani, A novel data augmentation based on Gabor filter and convolutional deep learning for improving the classification of COVID-19 chest X-Ray images, Biomedical Signal Processing and Control, Volume 72, Part A, 2022, 103326, ISSN 1746-8094, https://doi.org/10.1016/j.bspc.2021.103326.
32. Sinaga, Kristina & Yang, Miin-Shen. (2020). Unsupervised K-Means Clustering Algorithm. IEEE Access. PP. 1-1. https://doi.org/10.1109 ACCESS.2020.2988796
33. Holger R Roth, Ziyue Xu, Carlos Tor-Díez, Ramon Sanchez Jacob, Jonathan Zember, Jose Molto, Wenqi Li, Sheng Xu, Baris Turkbey, Evrim Turkbey, et al. (2022). Rapid artificial intelligence solutions in a pandemic - The COVID-19-20 Lung CT Lesion Segmentation Challenge. Medical image analysis, 82, 102605.
34. Lee S, Crawford MM. (2005). Unsupervised multistage image classification using hierarchical clustering with a Bayesian similarity measure. IEEE Trans Image Process, 14(3), 312-20. https://doi.org/10.1109/tip.2004.841195
35. Kenji Shimizu, Takeshi Johkoh, Junpei Ikezoe, Kazuya Ichikado, Jun Arisawa, Hironobu Nakamura, Shinichi Tamura, and Tomofumi Nagareda. (1997). Fractal analysis for classification of ground-glass opacity on high-resolution CT: an in vitro study. Journal of computer assisted tomography 21, 6 (1997), 955962.
36. R. Mahmoudi, N. Benameur, R. Mabrouk, M.A. Mohammed, B. Garcia-Zapirain, M.H. Bedoui, A deep learning-based diagnosis system for COVID-19 detection and pneumonia screening using CT imaging, Appl. Sci. 12 (10) (2022) 4825.
37. G. Wang, S. Guo, L. Han, A.B. Cekderi, Two-dimensional reciprocal cross entropy multi-threshold combined with improved firefly algorithm for lung parenchyma segmentation of COVID-19 CT image, Biomed. Signal Process. Control 78 (2022) 103933.

38. P.B. Chanda, S.K. Sarkar, Effective and reliable lung segmentation of chest images with medical image processing and machine learning approaches, in: 2020 IEEE International Conference on Advent Trends in Multidisciplinary Research and Innovation, ICATMRI, IEEE, 2020, pp. 1–6.
39. S. Guo, G. Wang, L. Han, X. Song, W. Yang, COVID-19 CT image denoising algorithm based on adaptive threshold and optimized weighted median filter, Biomed. Signal Process. Control 75 (2022) 103552.
40. W. Khan, N. Zaki, L. Ali, Intelligent pneumonia identification from chest x-rays: A systematic literature review, IEEE Access (2021).
41. Y.-H. Wu, S.-H. Gao, J. Mei, J. Xu, D.-P. Fan, R.-G. Zhang, M.-M. Cheng, Jcs: An explainable covid-19 diagnosis system by joint classification and segmentation, IEEE Trans. Image Process. 30 (2021) 3113–3126.
42. Y. Zhang, K. Chen, Y. Weng, Z. Chen, J. Zhang, R. Hubbard, An intelligent early warning system of analyzing Twitter data using machine learning on COVID-19 surveillance in the US, Expert Syst. Appl. (2022) 116882.
43. A. Banerjee, A. Sarkar, S. Roy, P.K. Singh, R. Sarkar, COVID-19 chest X-ray detection through blending ensemble of CNN snapshots, Biomed. Signal Process. Control (2022) 104000.
44. M.E. Sahin, Deep learning-based approach for detecting COVID-19 in chest X-rays, Biomed. Signal Process. Control (2022) 103977.
45. F. Al-Areqi, M.Z. Konyar, Effectiveness evaluation of different feature extraction methods for classification of covid-19 from computed tomography images: A high accuracy classification study, Biomed. Signal Process. Control 76 (2022) 103662.
46. S.H. Ahammad, M.Z.U. Rahman, A. Lay-Ekuakille, N.I. Giannoccaro, An efficient optimal threshold-based segmentation and classification model for multi-level spinal cord injury detection, in: 2020 IEEE International Symposium on Medical Measurements and Applications (MeMeA), IEEE, 2020, pp. 1–6.
47. J. Chen, C. Hef, J. Yin, J. Li, X. Duan, Y. Cao, L. Sun, M. Hu, W. Lia, Q. Lib, Quantitative analysis and automated lung ultrasound scoring for evaluating COVID-19 pneumonia with neural networks, IEEE Trans. Ultrason. Ferroelectr. Freq. Control (2021).
48. J. Hofmanninger, COVID-19 CT segmentation dataset, 2020, https://medicalsegmentation.com/covid19/.